G017

Resolving the Ambiguity in Attenuation Imaging

B. Hak (Delft University of Technology) & W.A. Mulder* (Shell International E&P BV)

SUMMARY

Seismic data enable imaging of the Earth, not only of velocity and density but also of attenuation contrasts. Unfortunately, the Born approximation of the constant-density visco-acoustic wave equation, which can serve as a forward modelling operator related to seismic migration, exhibits an ambiguity when attenuation is included. Different scattering models involving velocity and attenuation perturbations may provide nearly identical data. This result was obtained earlier for scatterers that did not contain a correction term for causality. Such a term will lead to dispersion when considering a range of frequencies. We demonstrate that with this term, iterative migration or linearised inversion will almost but not fully remove the ambiguity. Because the initial update in a gradient-based optimization scheme that minimizes the difference between modelled and observed data is still affected by the ambiguity, the reconstructed model starts to approximate the true model only after a very large number of iterations.

Introduction

Seismic imaging provides qualitative, structural information about the subsurface geology. Inversion – a term that we use in the mathematical sense of finding the Earth's parameters that best explain the observed data for a given type of forward modelling – leads to a quantitative description of material properties. Even with a simplified wave propagation model such as constant-density visco-acoustics, the reconstruction of not only the velocity but also the attenuation, as a function of subsurface position, can help in distinguishing between a fluid- or gas-filled rock formation.

Inversion for attenuation has been attempted by several authors with varying degrees of success. Ribodetti and Virieux (1998) considered linearised inversion for density, velocity, and attenuation perturbations in a given background model using ray tracing to model the wave propagation. The correction for causality was not included. They claimed successful reconstruction of the model perturbations, although their results have large errors near sharp interfaces. Hicks and Pratt (2001) and Smithyman et al. (2008), among others, consider the non-linear inversion problem. They appear to obtain good results with alternating updates of the velocity and the quality factor. Ribodetti et al. (2007) performed non-linear inversion in a VSP type configuration using synthetic data.

In an earlier paper (Mulder and Hak, 2009), we showed that an ambiguity occurs when performing linearised inversion with the constant-density visco-acoustic wave equation. In linearised inversion, the Born approximation for a given background model is used and the unknowns are the amplitudes of the scatterers. For the constant-density visco-acoustic wave equation, scattering is due to perturbations in the velocity as well as in the quality factor that measures the attenuation. We found that two different scattering models produce nearly identical seismic surface data. The same is true for any linear combination with relative weights summing to one. As a consequence, it will be impossible to recover both velocity and attenuation parameters for scatterers in this approach. In that paper, we used a model with a frequency-independent quality factor. The correction term required for causality was included for the background model but dropped in the scattering term, for simplicity. The question remains if the inclusion of this term in the scatterer will affect the occurrence of the ambiguity. The term introduces a frequency dependency that translates into dispersion. Will inversion over a sufficiently large bandwidth remove the ambiguity?

Theory

To answer that question, we consider the Born approximation of the constant-density visco-acoustic wave equation. The medium, including the scatterers, has slowness $\hat{\sigma}$ and quality factor $\hat{Q}$. Suppose the pressure wavefield $\bar{p}_s$ for source S is known for a background model with slowness $\bar{\sigma}$ and quality factor $\bar{Q}$. They both depend on position, although we will take them as constant in the example below. The total pressure wavefield in the Born approximation is then given by the sum of a background wavefield and a scattered wavefield p_s, which follow from

$$\big[-\omega^2\bar{m}(\omega)-\Delta\big]\bar{p}_s(\omega,\mathbf{x})=S(\omega,\mathbf{x}),\qquad \big[-\omega^2\bar{m}(\omega)-\Delta\big]p_s(\omega,\mathbf{x})=\omega^2 m(\omega,\mathbf{x})\,\bar{p}_s(\omega,\mathbf{x}).$$

Here $\omega=2\pi f$ is the angular frequency, and f is the frequency. The complex-valued parameters $\bar{m}$ and m are given by

$$\bar{m}(\omega)=\bar{\sigma}^2\big[1+(\mathrm{i}-a(\omega))\bar{Q}^{-1}\big],\quad m(\omega,\mathbf{x})=m^{(1)}(\mathbf{x})+(\mathrm{i}-a(\omega))m^{(2)}(\mathbf{x}),$$

where $a=(2/\pi)\log(f/f_r)$ is the causal correction term and f_r is a reference frequency against which causality is checked. The perturbation parameters $m^{(1)}=\hat{\sigma}^2-\bar{\sigma}^2$ and $m^{(2)}=\hat{\sigma}^2\hat{Q}^{-1}-\bar{\sigma}^2\bar{Q}^{-1}$ are both real-valued. For a source term $S=w_s(\omega)\delta(\mathbf{x}-\mathbf{x}_s)$, with a source wavelet $w_s(\omega)$ and a delta function at $\mathbf{x}_s$, the Born approximation leads to a scattered wavefield

$$p_{r(s)}=p_s(\omega,\mathbf{x}_r)=\omega^2\,w_s(\omega)\int d\mathbf{x}\;G(\omega,\mathbf{x}_s,\mathbf{x})m(\omega,\mathbf{x})G(\omega,\mathbf{x},\mathbf{x}_r),\tag{1}$$

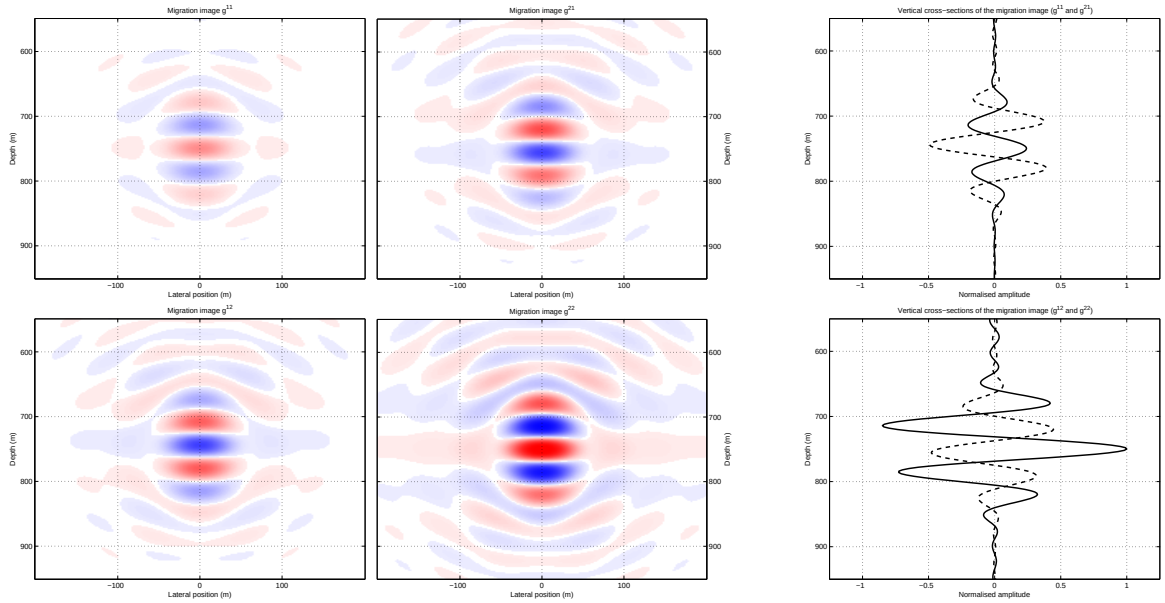

(a) (b)

Figure 1 *Resolution functions for a delta-function perturbation (a) and vertical cross-sections of the resolution function through the scattering point (b). The top row corresponds to a delta-function perturbation of the first model parameter, the bottom row to a delta-function perturbation of the second model parameter. In (a), positive values are red and negative blue. Ideally, the pictures on the top left and bottom right should resemble a band-limited version of a spike at the point-scatterer, as they do, and the other two pictures should have much smaller amplitudes, which they do not. In (b), the solid line represents the perturbed component, the dashed line is its contribution in the other component. The shape of this crosstalk, however, is rather different from the one obtained without the causal term, where there is a 90° phase difference. Here, the crosstalk has almost the opposite phase.*

where the background model $\bar{m}(\omega)$ determines the Green function $G(\omega, \mathbf{x}_1, \mathbf{x}_2)$, the wavefield at $\mathbf{x}_2$ due to a delta-function source at $\mathbf{x}_1$ or vice versa.

Earlier (Hak and Mulder, 2010), we assumed that $m(\omega, \mathbf{x}) \equiv m(\mathbf{x})$ by setting $a = 0$ in the scatterer only. In that case, equation (1) can be summarised as $\mathbf{p} = \mathsf{F}\mathbf{m}$, with a linear map F and using scalar complex values for the scattering model $m(\mathbf{x})$ and the data $p_{r(s)}$. The Hessian of the problem $\mathsf{H} = \sum_\omega \mathsf{F}^\dagger\mathsf{F}$ was Hermitian and $\mathsf{H}\,\delta(\mathbf{x} - \mathbf{x}_p)$ was the resolution function for a delta-function perturbation at position $\mathbf{x}_p$. The superscript $(\cdot)^\dagger$ denotes the conjugate transpose. If we do not ignore the causal term in the scatterer, we have to abandon the representation by complex-valued functions and treat the two real-valued parameters of the perturbation, $m^{(1)}$ and $m^{(2)}$, as separate model parameters. The inclusion of the dispersive term introduces a frequency dependency that breaks the symmetry between the real and imaginary part. This might alleviate the scattering ambiguity.

A new forward modelling operator $\tilde{\mathsf{F}}$ maps pairs $\{m^{(1)}(\mathbf{x}), m^{(2)}(\mathbf{x})\}$ to the data. This forward operator, together with the corresponding Hessian, can be expressed as

$$\begin{pmatrix} \mathrm{Re}\,\mathbf{p} \\ \mathrm{Im}\,\mathbf{p} \end{pmatrix} = \begin{pmatrix} \tilde{\mathsf{F}}^{11} & \tilde{\mathsf{F}}^{12} \\ \tilde{\mathsf{F}}^{21} & \tilde{\mathsf{F}}^{22} \end{pmatrix} \begin{pmatrix} \mathbf{m}^{(1)} \\ \mathbf{m}^{(2)} \end{pmatrix}, \quad \text{and,} \quad \mathsf{H} = \sum_\omega \tilde{\mathsf{F}}^{\mathsf{T}}\tilde{\mathsf{F}} = \begin{pmatrix} \mathsf{H}^{11} & \mathsf{H}^{12} \\ \mathsf{H}^{21} & \mathsf{H}^{22} \end{pmatrix},$$

respectively. The superscript $(\cdot)^{\mathsf{T}}$ denotes the transpose. All values are real. In this way, we obtain four resolution functions, one pair for a delta-function perturbation in a single point $\mathbf{x}_p$ of $m^{(1)}$ and one pair for $m^{(2)}$. The first pair corresponds mainly to a velocity perturbation and produces the resolution functions $\mathbf{g}^{11} = \mathsf{H}^{11}\delta(\mathbf{x} - \mathbf{x}_p)$ and $\mathbf{g}^{21} = \mathsf{H}^{21}\delta(\mathbf{x} - \mathbf{x}_p)$. The second pair corresponds to an attenuation perturbation and leads to the resolution functions $\mathbf{g}^{12} = \mathsf{H}^{12}\delta(\mathbf{x} - \mathbf{x}_p)$ and $\mathbf{g}^{22} = \mathsf{H}^{22}\delta(\mathbf{x} - \mathbf{x}_p)$.

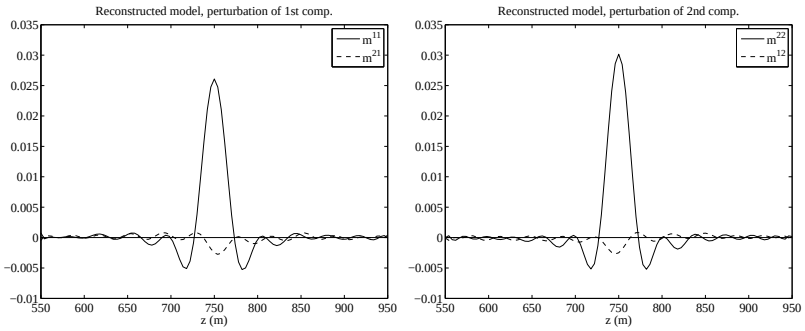

Figure 2 *Vertical cross-sections of the reconstructed perturbation through the scattering point. The left panel corresponds to a delta-function perturbation of the first component, the right panal to a perturbation of the second component. In both cases, a band-limited reconstruction is provided. A remnant in the wrong component is still present but is considerably smaller than in the case of a scatterer without a causal term.*

Ideally, $g^{11}(\mathbf{x})$ and $g^{22}(\mathbf{x})$ should resemble spikes at the position of the scatterer whereas $g^{21}(\mathbf{x})$ and $g^{12}(\mathbf{x})$ should be small. Least-squares inversion for the scatterer in a given background model that is kept fixed amounts to solving the linear problem

$$\mathsf{H}\,\mathbf{m} = \mathsf{H}\,\hat{\mathbf{m}}, \tag{2}$$

where $\hat{\mathbf{m}}$ is the true scatterer and $\mathbf{m}$ its reconstruction. As the Hessian H is singular, the linear system can be solved by means of the pseudo-inverse. This provides the minimum-norm solution. The system may also be solved by an iterative method that can handle its null-space, for instance, the conjugate-gradient method. Without preconditioning, this method should provide the minimum-norm solution. With preconditioning, the usual norm is replaced by a weighted norm, determined by the preconditioner, and the solution of the singular problem will differ from the one obtained without preconditioning.

Results

We consider the same example as before (Hak and Mulder, 2010): a point scatterer in a 2D constant background model with velocity $c_0 = 2$ km/s and quality factor $Q = 100$. The scatterer is located at $x = 0$ and $z = 750$ m. Sources are placed between -1887.5 and $+1887.5$ m at a 25-m interval and receivers between -1900 and $+1900$ m at the same interval, all at zero depth. We computed the Hessian on a grid with 101×101 points and a spacing of 4 m, having the scatterer at the centre. This resulted in a Hessian matrix of size 20402×20402. We used a Ricker wavelet with a peak frequency of 15 Hz and considered frequencies in the range between 4 and 20 Hz at a 0.5-Hz interval.

Figure 1(a) shows the resolution functions. A delta-function perturbation of the first component produces a band-limited version, g^{11}, after migrating the data, but also produces substantial crosstalk in the other component, g^{21}, with an even larger amplitude. A delta-function perturbation of the second component has a migration image for the second component, g^{22}, that looks reasonable, but again there is significant crosstalk, g^{12}, which now has a smaller amplitude. Figure 1(b) displays vertical sections through the scatterer point of the resolution functions for a delta-function perturbation of the first and second component. Compared to the case of a scatterer without causal correction term, presented elsewhere (Hak and Mulder, 2010), we note that the crosstalk into the wrong component is still substantial, but now has a phase difference of almost 180° instead of 90°.

Because the crosstalk is still large, simultaneous imaging of velocity and attenuation perturbations will lead to erroneous results if just a single step is carried out. However, if we try to solve equation (2) by iterative migration, the result may improve. In the current example, we directly computed the pseudo-inverse of the Hessian and obtained the reconstructions shown in Figure 2. The left panel displays a vertical section obtained for a delta-function perturbation of the first component, the right panel for a

perturbation of the second. The inversion has considerably reduced the amount of crosstalk and provided an acceptable band-limited reconstruction of the scatterer.

The results show that inclusion of the frequency-dependent causal correction term in the scatterer provides sufficient additional information to enable a better reconstruction. This agrees with the work of Innanen and Weglein (2007). However, in a iterative migration approach, the substantial crosstalk in the first iteration suggests that a large number of iterations will be required before the crosstalk is reduced to an acceptable level. Indeed, we found that the solution of equation (2) by a conjugate-gradient method without preconditioning took 11445 iterations for a decrease of the residual by a factor 10^{-7} to obtain the same result as in Figure 2. The number was reduced to 8016 iterations by preconditioning with a diagonal matrix that has 1 on the diagonal for the first unknown, $m^{(1)}$, and $\bar{Q}$ for the second unknown, $m^{(2)}$, at each grid point. This is still substantial and too large to be of practical use in applications of iterative migration (Østmo et al., 2002; Mulder and Plessix, 2004).

Conclusions

We have investigated if the inclusion of the correction for causality in the scatterer circumvents the ambiguity that occurs for attenuation scattering imaging based on the Born approximation. By including this causality we introduce a frequency-dependent dispersion term. When using a range of frequencies, this term almost, but not completely, removes the ambiguity that otherwise occurs between the real and imaginary parts of the scattering model.

The initial update of a gradient-based optimisation algorithm that tries to minimise the difference between modelled and observed data differs significantly from the correct update. Many iterations are therefore required to approach the true solution. This implies that, although dispersion allows us to resolve the ambiguity in attenuation imaging in the example considered here, it will be difficult to actually find the true model in realistic cases when noise is present and the number of iterations has to be limited because of computational cost.

Acknowledgements

This work is part of the research programme of the 'Stichting voor Fundamenteel Onderzoek der Materie (FOM)', which is financially supported by the 'Nederlandse Organisatie voor Wetenschappelijk Onderzoek (NWO)'.

References

Hak, B. and Mulder, W.A. [2010] Migration for velocity and attenuation perturbations. *Geophysical Prospecting*, (in press).

Hicks, G.J. and Pratt, R.G. [2001] Reflection waveform inversion using local descent methods: Estimating attenuation and velocity over a gas-sand deposit. *Geophysics*, **66**(2), 598–612.

Innanen, K.A. and Weglein, A.B. [2007] On the construction of an absorptive-dispersive medium model via direct linear inversion of reflected seismic primaries. *Inverse Problems*, **23**(6), 2289–2310.

Mulder, W.A. and Hak, B. [2009] An ambiguity in attenuation scattering imaging. *Geophysical Journal International*, **178**(3), 1614–1624.

Mulder, W.A. and Plessix, R.E. [2004] A comparison between one-way and two-way wave-equation migration. *Geophysics*, **69**(6), 1491–1504.

Østmo, S., Mulder, W.A. and Plessix, R.E. [2002] Finite-difference iterative migration by linearized waveform inversion in the frequency domain. SEG 72nd Annual Meeting, Salt Lake City (UT), USA, Expanded Abstracts, 1384–1387.

Ribodetti, A., Plessix, R.E., Operto, S. and Virieux, J.M. [2007] Viscoacoustic frequency-domain full-waveform inversion – application to numerical VSP data. 69th EAGE Conference & Exhibition incorporating SPE EUROPEC, London, GB, Extended Abstracts, C029.

Ribodetti, A. and Virieux, J. [1998] Asymptotic theory for imaging the attenuation factor Q. *Geophysics*, **63**(5), 1767–1778.

Smithyman, B.R., Pratt, R.G., Hayles, J.G. and Wittebolle, R.J. [2008] Near surface void detection using seismic Q-factor waveform tomography. 70th EAGE Conference & Exhibition incorporating SPE EUROPEC, Rome, Italy, Extended abstract, F018.